Current Biology 20, 423–428, March 9, 2010 ©2010 Elsevier Ltd All rights reserved DOI 10.1016/j.cub.2009.12.056

Report

# A "Primer"-Based Mechanism Underlies Branched Actin Filament Network Formation and Motility

Vérane Achard,[1,3] Jean-Louis Martiel,[2,3] Alphée Michelot,[1,4] Christophe Guérin,[1] Anne-Cécile Reymann,[1] Laurent Blanchoin,[1,*] and Rajaa Boujemaa-Paterski[1,*]
[1]Laboratoire de Physiologie Cellulaire Végétale, Institut de Recherches en Technologies et Sciences pour le Vivant, CNRS/CEA/INRA/UJF, 38054 Grenoble, France
[2]Laboratoire Techniques de l'Ingénierie Médicale et de la Complexité, CNRS/UJF, Pavillon Taillefer, Faculté de Médecine, 38706 La Tronche, France

## Summary

**Cells use actin assembly to generate forces for membrane protrusions during movement [1] or, in the case of pathogens, to propel themselves in the host cells, in crude extracts [2], or in mixtures of actin and other purified proteins [3]. Significant progress has been made in understanding the mechanism of actin-based motility at a macroscopic level by using biomimetic systems in vitro [4–6]. Here, we combined such a system with evanescent wave microscopy to visualize Arp2/3-mediated actin network formation at single-actin-filament resolution. We found that actin filaments that we call "primers" determine the origin of the autocatalytic and propagative formation of the actin network. In the presence of capping protein, multiple "primers" generate independent networks that merge around the object to form an outer "shell" made of entangled and capped filaments. Simultaneously, newly created filaments on the surface of the particle initiate mechanical stress, which develops until symmetry breaking. Our results and extensive modeling support that the stress, which releases into propulsive forces [7], is controlled not by any specific orientation of actin filaments toward the nucleation sites but only by new monomers added near the load surface.**

## Results and Discussion

### Experimental Design

We used total internal reflection fluorescence microscopy (TIRFM) to study the dynamic formation of Arp2/3 complex branched actin networks in real time at single-actin-filament resolution. We followed actin assembly around 10–40 μm glass rods coated with pWA, the C-terminal region of WASP/Scar protein [8] that initiates actin polymerization in the presence of Arp2/3 complex and G-actin. The initial steps of actin assembly and the network extension around the particles were characterized with Alexa 488-labeled G-actin [9]. Additionally, the use of photosensitive Alexa 532-labeled actin allowed us to track individual actin filaments during the polymerization within such a dense and branched actin network. Therefore, we were able to monitor in real time the sustained and autocatalytic branch formation, which continuously propagates along the particle surface.

### Actin Filament "Primers" Are Necessary to Initiate Arp2/3 Complex-Mediated Actin Polymerization around the NPF-Coated Particle

As a first step, and because nonmuscle cells maintain unpolymerized actin at concentrations as high as 100–300 μM, we used a profilin-G-actin buffered medium containing a minimal set of purified actin-binding proteins to reconstitute sustained actin-based motility of nucleation-promoting factor (NPF)-coated beads and glass rods. The recorded velocities were 8–33 nm/s (Figures 1A and 1B; see also Movies S1A and S1B available online). In these conditions where the actin monomer pool is bound to profilin, actin filaments nucleated by Arp2/3 complex elongate strictly at free barbed ends. Although this macroscopic reconstitution under physiological conditions was an important step toward identifying the nature of the minimal set of purified proteins essential to generate actin-based motility, most of the molecular mechanisms involved in building the actin filament meshwork remain to be established.

Using evanescent wave microscopy, we observed specifically the elementary molecular reactions that control actin dynamics leading to symmetry breaking and motility at a microscopic level and addressed the central role of heterodimeric capping protein (CP; the muscle isoform is also called CapZ) in these processes. We first investigated how assembly of actin filaments at the surface of NPF-coated particles is initiated. We discovered that NPF-coated particles only induced autocatalytic actin assembly after an initial contact with a drifting actin filament in the medium (Figure 1C, red and green arrowheads; Movie S1C) or with an actin filament emanating from an adjacent branched network (Figure S1A; Movie S1D), which is consistent with biochemical measurements [8]. Accordingly, the time to first contact between the NPF-coated particles and a drifting actin filament decreases as a function of the density of "primers" in solution (Figure 1D). The observation of this activation by a drifting "primer" responsible for the initiation of protruding actin networks was buried because of the high concentration of actin filaments present in the media of reconstituted systems used previously [2–5]. Moreover, the long functionalized rods allowed us to observe that several actin filament "primers" were required to achieve the rapid and overall spread of an actin-branched network around the particle (Figure 1C). We found that the actin-branched network often drifted around the NPF-coated glass fiber, contacted the rod, initiated branches, and finally detached, so the interactions of filaments with the nucleation sites on the fiber were transient (Figure 1E; Movie S2A); this was consistent with biochemical measurements of rapid dissociation of VCA from Arp2/3 complex [10].

### Barbed Ends of Branched Actin Filaments Initiated at the Nucleation Sites Grow away from the NPF-Coated Particle

To further characterize the geometry of the branched network of actin filaments assembled at the surface of

*Correspondence: laurent.blanchoin@cea.fr (L.B.), rajaa.paterski@cea.fr (R.B-P.)
[3]These authors contributed equally to this work
[4]Present address: Department of Molecular & Cell Biology, University of California, Berkeley, Berkeley, CA 94720-3202, USA

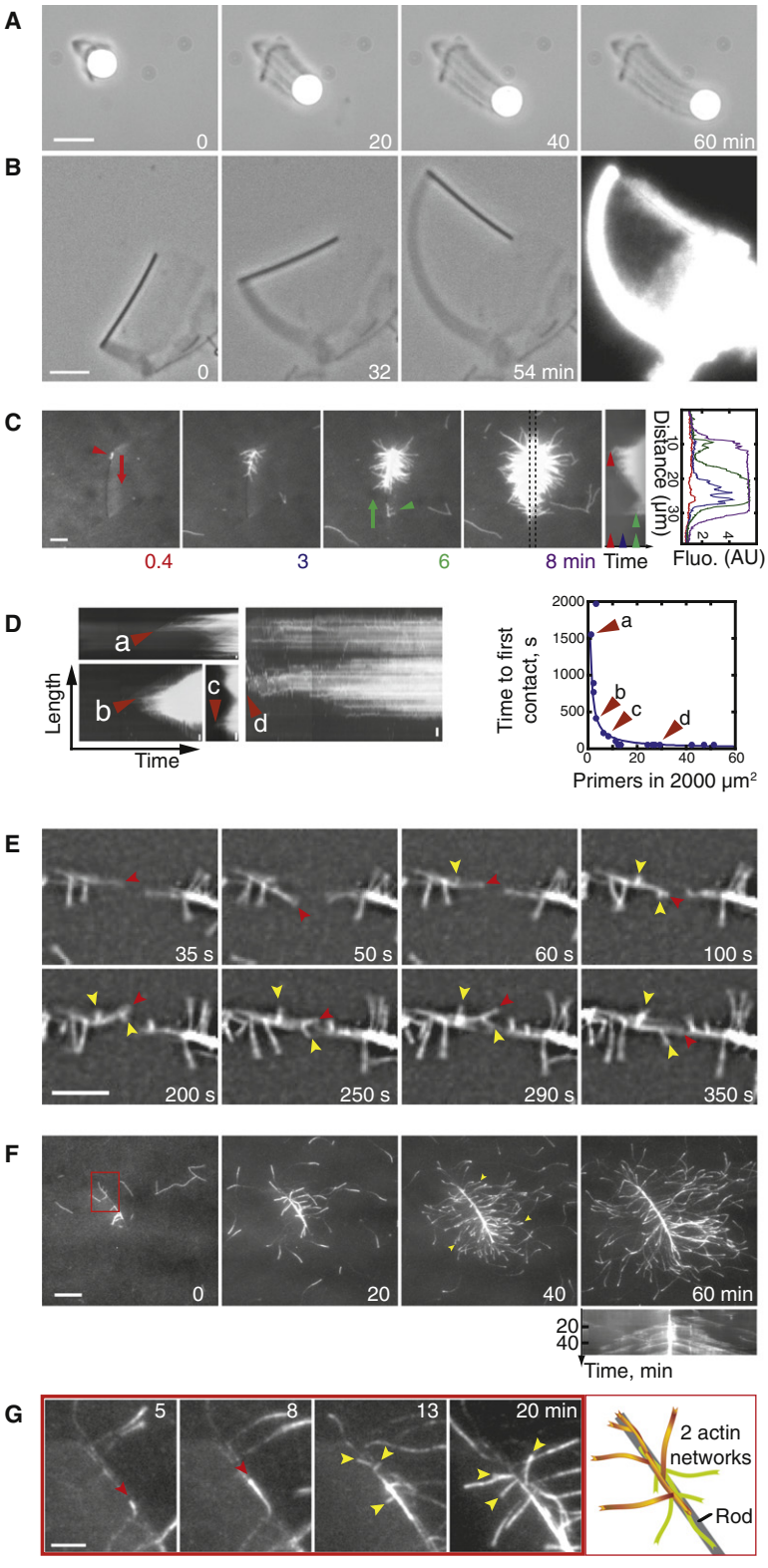


Figure 1. Dynamic Architecture of an Arp2/3 Complex-Generated Actin Filament Network

(A and B) Reconstituted motility of 2 μM GST-pWA-coated beads or 9 μM GST-pWA-coated rods, imaged by phase-contrast microscopy, with 4 μM G-actin, 12 μM profilin, 75 nM Arp2/3 complex, 25 nM capping protein (CP), and 1 μM ADF/cofilin. G-actin was 7% Alexa 488 labeled. Epifluorescence image highlights the actin network density.

(C–F) Actin assembly around nucleation-promoting factor (NPF)-coated particles followed by total internal reflection fluorescence microscopy (TIRFM).

(C) Actin filament triggers polymerization around 1 μM GST-pWA-coated rods with 50 nM Arp2/3 complex and 1.2 μM Alexa 488-G-actin. Red and green arrowheads indicate initial contact of an actin filament "primer" with the particle, and arrows show the direction of actin filament elongation. Kymographs, measured between the dotted lines, illustrate the fluorescence increase due to polymerization; corresponding fluorescence intensity distribution was calculated at different times. Color coding in graph at right is associated with times indicated by colored numbers under panels to the left.

(D) Actin polymerization around NPF-coated rods was analyzed (in conditions similar to C), and the time to first contact by a "primer" was determined for different densities of filaments measured in the evanescent wave field (2000 μm$^2$). The spontaneous nucleation process of monomeric actin in the reconstituted medium was tuned with increasing amount of profilin. The actin filament "primers" that initiate actin assembly along the glass rod range between 1 and 2 μm in length. Kymographs illustrate the fluorescence increase due to polymerization. (a)–(d) represent activation events. The graph at right represents the comparison between experimental results (blue dots) and the theoretical prediction (solid line) based on a diffusion-controlled capture of "primers" by rods [16].

(E) 0.5 μM Alexa 532-G-actin polymerized in the presence of 1.5 μM profilin, 0.5 μM ADF/cofilin, and 33 nM Arp2/3 complex into actin filaments (red arrowheads) that initiate branches (yellow arrowheads) on 0.5 μM GST-pWA-coated rods.

(F) Actin network assembly on 5 μM GST-WA-coated rods mixed with 0.8 μM Alexa 532-G-actin and 40 nM Arp2/3 complex; kymograph highlights branching activity emerging from the rod.

(G) Zoomed region of actin network indicated by red box in (F) (color code as in E). The cartoon at right represents the two actin networks generated on the rod.

Scale bars represent 5 μm. (See also Figure S1 and Movies S1 and S2.)

functionalized glass rods by Arp2/3 complex, we followed the growth of the network by using G-actin covalently labeled with Alexa 532. Rapid photobleaching of polymerized Alexa 532-actin allows one to follow barbed ends elongating either outwards or, interestingly, within the branched network, because they are much brighter than older regions of the filaments [11]. Whereas previous studies described actin incorporation sites around motile particles by static labeling of the branched actin network or by speckle microscopy [12, 13], here we monitored actin filament network formation in real time at single-actin-filament resolution and obtained a chronological description of the elementary events that lead to actin-based motility. We found that the actin-branched network elongated with all barbed ends growing away from the NPF-coated glass rod (Figure 1F; Movie S2B; see also Figure S1B for modeling), subsequent to the stimulation of Arp2/3 complex branching activity on actin filaments growing along the NPF-coated rod (Figure 1G; Movie S2C).

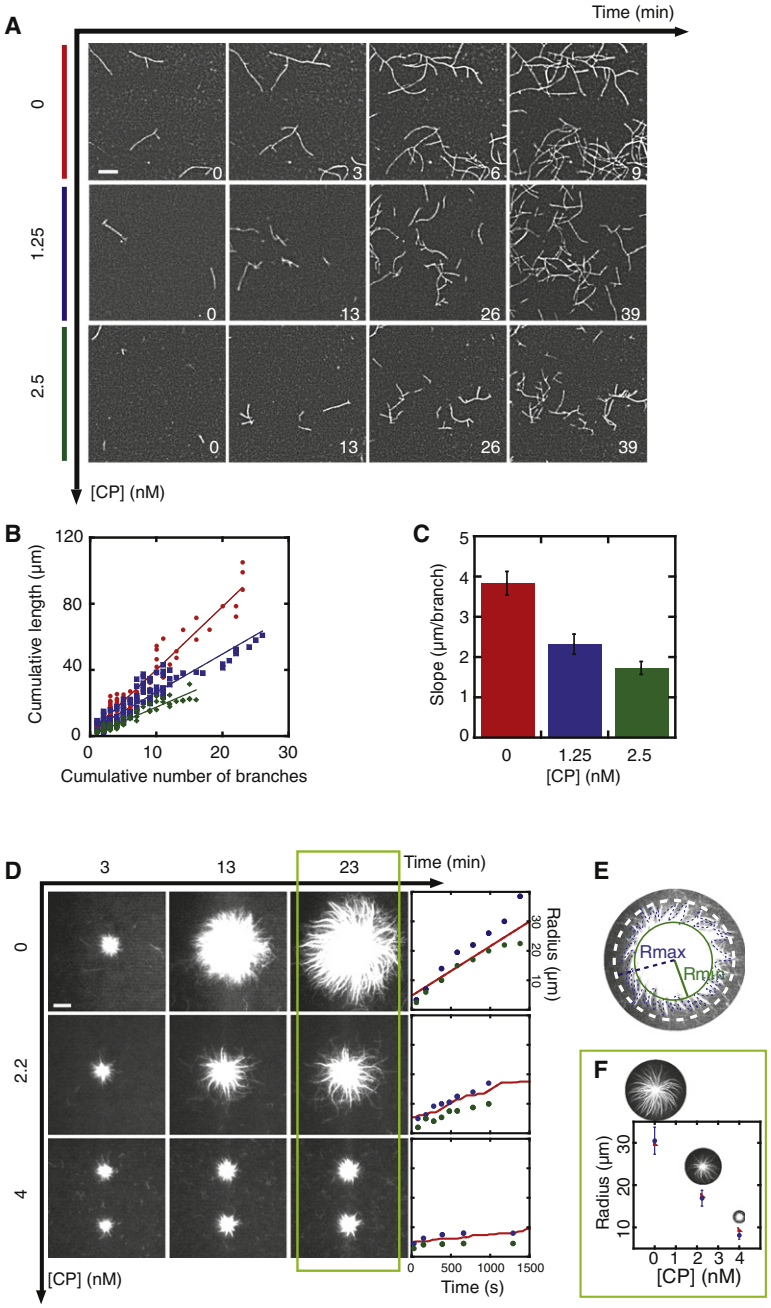


Figure 2. Capping Protein Limits the Average Network Extension Radius around Particles by Reducing the Average Branch Length

(A) Dynamic assembly of actin-branched structures in solution observed by TIRFM with 1 μM Alexa 568-G-actin, 10 nM Arp2/3 complex, 113 nM GST-WA, and CP at the indicated concentrations.

(B) The total number of branches counted correlates linearly with the cumulative length (dots) as predicted by simulation (lines).

(C) The average filament length is reduced with increasing CP concentration. Error bars are the error of each slope calculated from the linear regressions in (B).

(D) Decrease of the radius of actin networks around 4 μM GST-WA-coated beads with 1.5 μM Alexa 532-G-actin, 30 nM Arp2/3 complex, and CP at the indicated concentrations; each reaction was followed by TIRFM. Rightmost column: comparison between the experimental actin network radius around beads versus time (blue dots = $R_{max}$, green dots = $R_{min}$) and in silico simulation (solid line) (see Figure S1C and Supplemental Experimental Procedures).

(E) Cartoon illustrating the $R_{max}$ and $R_{min}$ determination.

(F) Experimental (blue dots) and simulated (red triangles) mean actin network radius decreases with CP concentration (n = 20 for each condition). Error bars represent the standard deviation of the radii measured for each CP concentration.

Scale bars in (A) and (D) represent 5 μm. (See also Figure S1.)

## Capping Protein Shortens the Growth of Actin Filament "Primers" and Creates Independent Networks around the NPF-Coated Particle

We investigated the role of CP in the architecture of a growing Arp2/3 complex-mediated actin network prior to symmetry breaking. CP was identified as one of three actin-binding proteins (ABPs) that precisely choreograph actin polymerization and organization to generate "comet tail" motility in vitro [3]. Heterodimeric CP binds with high affinity (0.1 nM) to filament barbed ends and prevents subunit loss or addition. First, we followed Arp2/3 complex-mediated branch formation in solution (Figure 2A) to quantify the kinetic formation of a dendritic filament network (Figure 2B; Figure S1C). Both the total number of branches and their cumulative length increased exponentially over time. Increasing CP concentration did not affect this autocatalytic behavior but reduced the average filament length (Figure S1C). As a consequence, the average distance between two branching points on a mother branch was negatively correlated with increasing CP concentration as a result of less available actin filament length to host the nucleation of new branches (Figure 2C). Second, when NPFs were located on beads or glass rods, increasing the concentration of CP reduced the radius of the actin network assembled around the particle (Figures 2D and 2E), in agreement with our kinetic model implemented with the capping activity (Figure 2F; Supplemental Experimental Procedures).

Capping actin filament barbed ends constrained actin filament elongation near the NPF nucleating sites (Figure 2D; Figure 3B; Figure S2C), in agreement with previous studies [6, 12], but without necessarily affecting the orientation of branches in the network assembled around particles. To increase the spatial resolution, we followed Arp2/3 complex-mediated actin-branched network assembly around glass rods, instead of around beads, with Alexa 532-actin monomers. The branched actin filaments grew away from the rod until being capped at their barbed end (Figure 3A). Using photobleaching of Alexa 532-actin, we followed the elongation of new fluorescent actin branches until they disappeared after a capping event (Figure 3A; Movie S3A). When the CP concentration was increased, the actin-branched network did not propagate efficiently along the rod (Figure 3C). In order to obtain a homogenous spread of branched filament network along the functionalized rod, actin assembly must be initiated by multiple actin filament "primers" at several NPF coating sites (Figure 3C).

We simulated the kinetics of nucleation, branching, and capping of new filaments on glass rods (Figure 3D; Movie

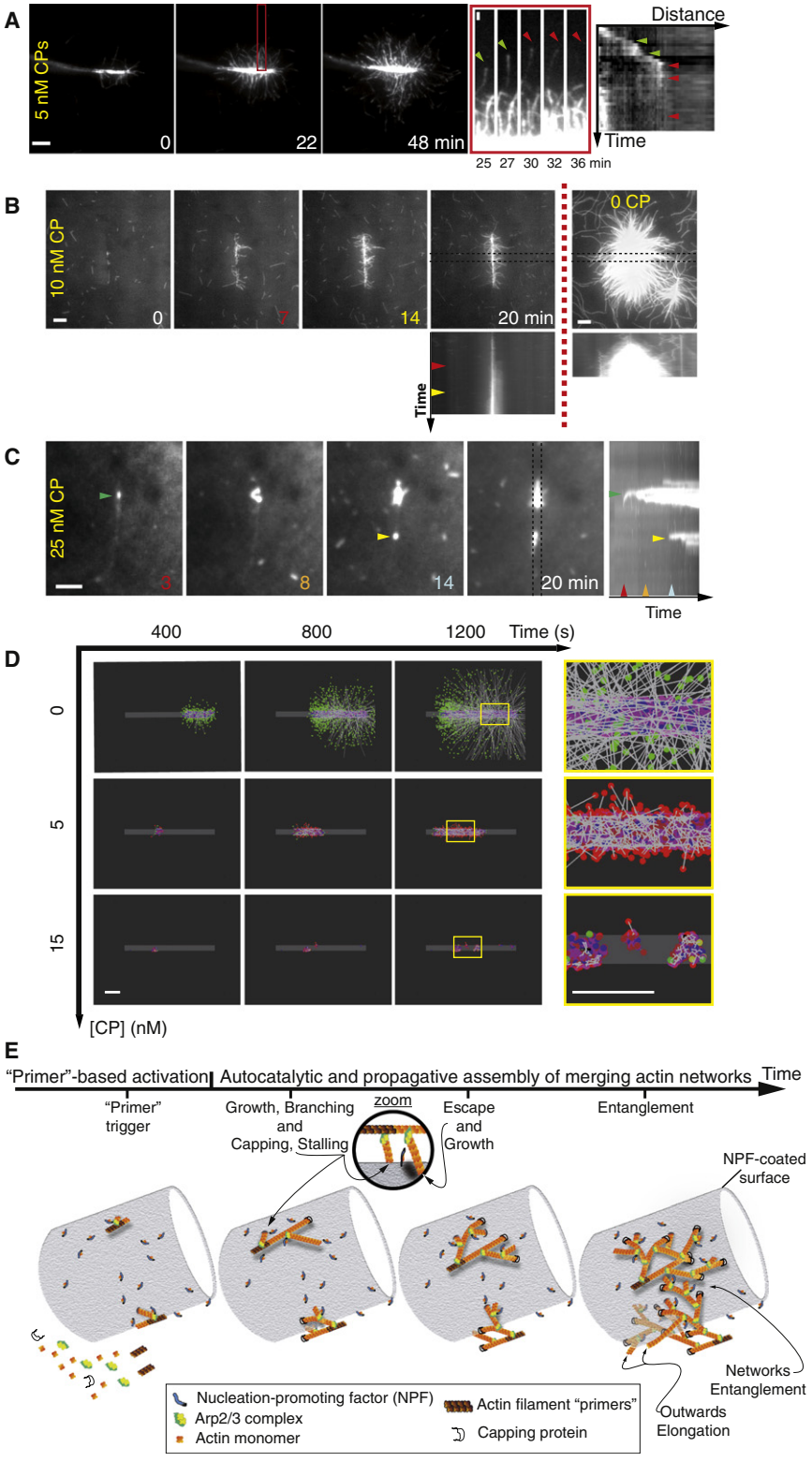


Figure 3. Spreading of Actin-Branched Network along Glass Rods Emanates from Actin Filament "Primers" and Is Limited by Capping Protein

(A–C) Actin assembly is followed by TIRFM. Scale bars represent 5 μm.

(A) 0.8 μM Alexa 532-G-actin polymerizes around 5 μM GST-WA-coated glass rods with 80 nM Arp2/3 complex and 5 nM CP. Barbed ends grew away from the rod (green arrowheads) before been capped (red arrowheads). The fluorescence of the Alexa 532 then disappears as a result of photobleaching, as shown in the zoom of the red boxed area and in its associated kymograph.

(B and C) 2 μM Alexa 488-G-actin polymerizes around 1 μM GST-pWA-coated glass rods with 25 nM Arp2/3 complex and CP as indicated. Arrowheads indicate the contact of the initial actin filament "primer" with the NPF-coated particle. The color code used in the kymographs in (B) and (C) is associated with the indicated times.

(D) Simulated network growth. Activated Arp2/3 complex (magenta dots) initiates branches (gray lines) on the actin filament "primers." Free barbed ends (green dots) escape the rod surface or are stalled against it (blue dots). However, because of thermal fluctuations, stalled barbed ends are oriented tangentially to the particle surface. Thereby, actin filament barbed ends resume their growth (yellow dots). In the presence of CP, the spatial actin network extension is reduced (capped barbed ends; red dots). The rightmost column magnifies the yellow boxed regions of each row. Scale bars represent 10 μm.

(E) Model of branched network formation around the motile particle. The molecular mechanism of Arp2/3 complex-mediated network formation consists of an initial "primer"-based activation ("primer" trigger step) followed by the autocatalytic and propagative spread of the network. Each "primer" creates an independent network. These networks merge to cover the particle. Each new branch can transiently be stalled against the load (see Figure S2Ab and [17]) or elongate away from it before being capped. Networks are viewed from the top. The encircled area at top is a zoomed side view of some branching points. (See also Figure S2 and Movie S3.)

S3B) or beads (Figures 2D–2F) by using the different kinetic steps illustrated in Figure 3E (see also the detailed description of the model in Supplemental Experimental Procedures and Figures S2A and S2B). Based on the experimental settings in which neither the density of NPFs nor the concentrations of Arp2/3 complex or actin monomers were limiting, nucleation of new filament branches was a self-sustained process that depended on CP concentration (Figure 3D; Movie S3B). Barbed-end capping restricted the maximal growth of the network, whereas it had little or no effect on the self-sustained nucleation process at low CP concentration (Figure 3D; Movie S3B). Additionally, capping modified the distribution of filament branch lengths, but barbed-end orientation remained isotropic. Because CP reduced the average filament length, both the network radius and the rate of network extension were smaller with than without CP. Moreover, CP increased the density of actin filaments inside the network. The model shows that a single actin filament "primer" was sufficient at low CP concentration to trigger an explosive generation of branches (Figure 3D, top and middle panels;

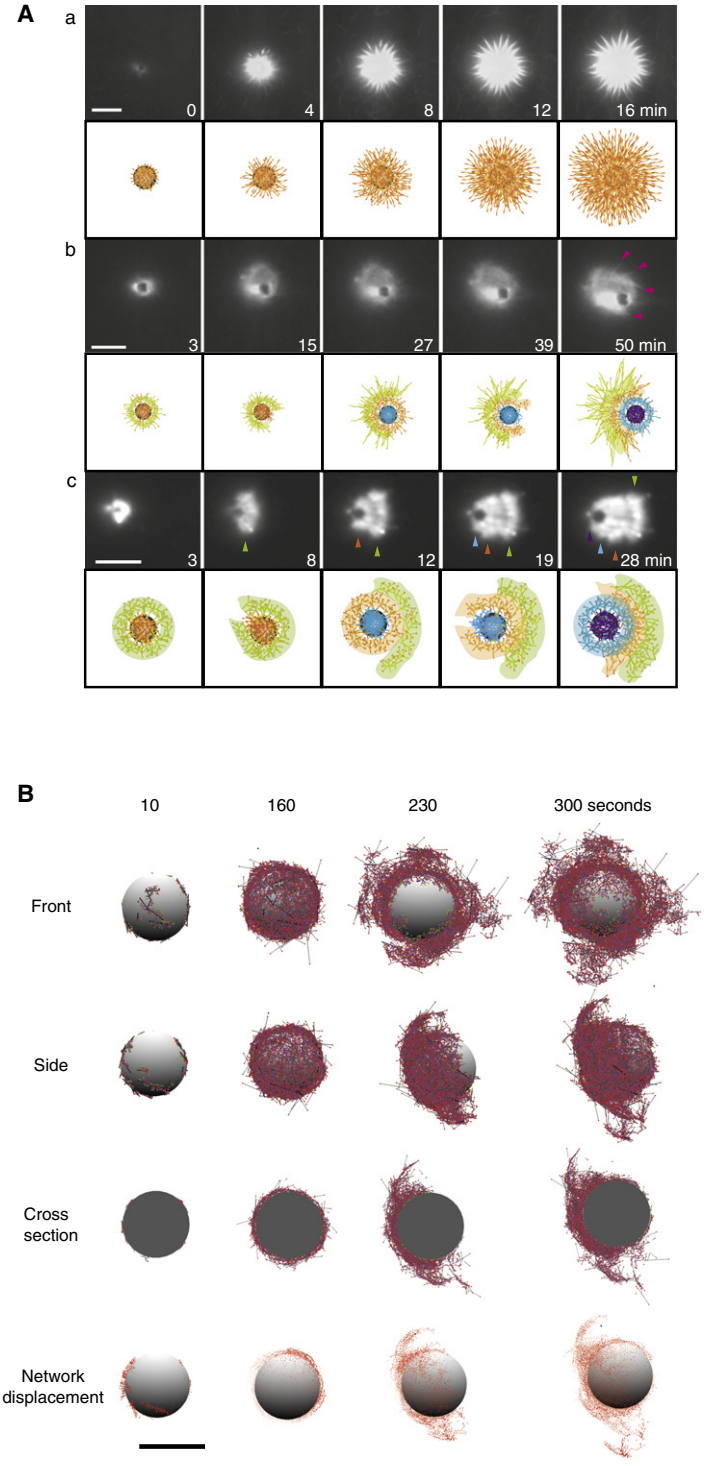


Figure 4. Network Rupture Occurs through a "Multiple Shell-Breaking" Process of Randomly Oriented Actin Filaments

(Aa–Ac) An isotropic actin network assembles around 2 μM GST-pWA-coated beads mixed with 2 μM Alexa 488-G-actin and 50 nM Arp2/3 complex (Aa). Addition of 25 nM CP triggers a "multiple shell-breaking" process (Ac); arrowheads indicate the successive shells. We changed the ratio of Arp2/3 complex to CP and still observed the multiple shell-breaking process for 4 μM GST-pWA-coated beads mixed with 4 μM Alexa 488-G-actin, 12 μM profilin, 100 nM Arp2/3 complex, and 25 nM CP. However, insufficient capping leads to a "fishbone" pattern in the actin "comet" (Ab). Arrowheads highlight elongating filaments or bundles growing away from the bead. Scale bars represent 10 μm.

(B) Under the experimental conditions in (Ac), the model (see Supplemental Experimental Procedures) shows that after an isotropic and homogeneous growth of filaments nucleated on the bead (10–170 s), the internal stress fractures the network (170 s) before the filaments are displaced (between 170 s and 230 s). Newly nucleated actin filaments spread over the bead "empty zone" (after 230 s), leading to the reconstruction of a fully developed network. The free barbed ends in the network that move away from the bead (170–230 s) are rapidly capped and form the "comet tail." Scale bar represents 5 μm. (See also Figures S2 and S3 and Movies S4 and S5.)

Movie S3B). Conversely, experimental data and numerical simulations showed that above a CP concentration of ~10 nM (in our experimental setup), the shortened actin filament "primers" and reduced duration of branch elongation were unable to sustain autocatalytic branching (Figures 3C and 3D, bottom panel; Movie S3B). For CP concentrations above 10 nM, the model predicts that up to 20 independent actin filament "primers" were necessary to generate a fully developed filament meshwork comparable to experimental data (Figure 1; Figure 4).

### Evidence for a "Multiple Shell-Breaking" Process during Actin-Based Motility

To bridge the molecular events of actin filament meshwork formation and actin-based motility of NPF-coated beads, we used evanescent wave microscopy to follow actin assembly around particles until symmetry breaking. In the absence of CP, functionalized beads assembled an actin network with a star-like pattern, as Arp2/3 complex-nucleated branches at the bead surface with their barbed ends growing away from the bead (Figure 4Aa). Surprisingly, in the presence of sufficient CP, we found that sustained motility results from a "multiple shell-breaking" process (Figure 4Ac; Movie S4B) during "continuous movement" observed by phase contrast or epifluorescence microscopy (Figures 1A and 1B).

Based on this observation, we propose the following model centered on the control of actin filament length by CP (Figure S2C): (1) CP creates a "dead zone" at the outer actin "shell" by inhibiting all actin filament elongation beyond the shell radius; (2) Arp2/3 nucleation occurs strictly at the bead surface because NPF is immobilized on the particle; this will create an active polymerization zone embedded within the constrained dead zone; (3) continuous actin nucleation in the vicinity of the bead will generate an internal stress that breaks the former dead zone; and (4) CP will block elongation of actin filaments in the "active zone," creating a new dead zone, while Arp2/3 complex nucleates new actin filaments at the surface of the bead, building a new active zone. The dead zone breaking repeats, leading to the multiple shell-breaking process. The existence of cyclic versus continuous network breakage was assigned to different mechanisms controlled by either particle size [5] or the role of fluctuations behind symmetry breaking [6, 14]. Based on our observations, we propose that the actin network oscillates between expansion and rupture phases, but depending on the network thickness at rupture, this process may or may not be observable via conventional microscopy methods but is always observable via TIRFM.

Moreover, when the ratio between Arp2/3 complex and CP is low, multiple shell breaking still occurs, but some actin

filaments elongate beyond the dead shell radius (Figure 4Ab; Figure S2C; Movie S4A), giving rise to the "fishbone" pattern observed previously [15].

### Symmetry Breaking: The Elastic Continuum Made of Elementary Merging Actin Meshworks Breaks upon Mechanical and Spatial Constraints

We modeled dynamic organization of actin filaments during network formation and shell breakage (Supplemental Experimental Procedures). Simulations presented in Figure 3 show that when the CP concentration is high ( ~ 25 nM; see Figure 4A), about 30 independent "primers" are required to generate full coverage of the bead by growing actin filaments. Extension and merging of these elementary networks (Figure 3E; Figure S2E), each generated by a single "primer" filament, provides a continuous tiling of the bead within ~ 30 min (Figure 4B; Movie S5). Extension of this network is accompanied by a slow but constant displacement of the actin filaments away from the bead (Figure 3E; Figure 4B; Movie S5). However, because entanglements between networks tend to oppose the forces generated at the bead surface, the progression of the network slows down and it reaches equilibrium. At 170 s, thermal fluctuations lead to the uniform tiling rupture by moving the filaments away from the bead and leaving an empty space (Figure S2E). This rapid movement (between 180 s and 230 s) relieves the stress applied to the actin filaments, which in turn results in a marked increase in the generation of new filaments (Figure S2Fa). However, the orientation of actin filaments remains isotropic (Figure S2Fc). The occurrence of symmetry breaking of the actin filament network around a NPF-coated bead in the presence of a high concentration of Arp2/3 complex and in the absence of CP (Figure S3) confirms our model's fundamental hypothesis of barbed-end steric constraint.

### Concluding Remarks

We propose that Arp2/3 complex-mediated force generation is based on a simple but fundamental steric constraint wherein elongating barbed ends tend to escape when they are aimed directly at the load and simultaneously entangled into a broad actin meshwork. Thus, filaments either growing along the load or growing outwards create a steric hindrance and a stress, which releases into propulsive forces, consistent with the mechanics of symmetry breaking of actin gel [6, 7]. Therefore, a challenge for future investigations will be to constrain our molecular model with previous observations on the symmetry breaking time [7] to predict at the molecular level the mechanical properties of the active gel around the motile particle.

We have demonstrated that actin filaments that we call "primers" initiate the formation of the actin network. Physiological concentration of capping proteins shortens the growth of these "primers" and creates independent networks made of isotropically oriented actin filaments that merge around the motile particle. Moreover, the movement of NPF-coated particles then results from a multiple shell-breaking process controlled by the tight tiling of these independent networks, each grown from a single actin filament "primer." Our observations suggest that force production necessary to propel cytoplasmic particles or to protrude the plasma membrane relies not necessarily on any preferential orientation of actin filaments inside the network, but on simple and universal physics laws. The "primer"-based mechanism likely emerges as a general feature of branched network assembly involved in "comet tail" or lamellipodium formation during pathogen or cell motility. Based on this mechanism, actin filaments parallel to the nucleating surface constitute an efficient and optimal way to initiate branched network formation upon signaling.

#### Supplemental Information

Supplemental Information includes Supplemental Experimental Procedures, three figures, and five movies and can be found with this article online at doi:10.1016/j.cub.2009.12.056.

#### Acknowledgments

We are grateful to T.D. Pollard, J. Van der Gucht, J.-F. Joanny, C.J. Staiger, and D. Vignjevic for helpful discussions and insightful suggestions. This work was supported by Agence Nationale de la Recherche grant ANR-06-PCV1-0022 to L.B. and J.-L.M.

Received: October 1, 2009
Revised: December 22, 2009
Accepted: December 23, 2009
Published online: February 25, 2010

#### References

1. Pollard, T.D., and Borisy, G.G. (2003). Cellular motility driven by assembly and disassembly of actin filaments. Cell *112*, 453–465.
2. Cameron, L.A., Giardini, P.A., Soo, F.S., and Theriot, J.A. (2000). Secrets of actin-based motility revealed by a bacterial pathogen. Nat. Rev. Mol. Cell Biol. *1*, 110–119.
3. Loisel, T.P., Boujemaa, R., Pantaloni, D., and Carlier, M.F. (1999). Reconstitution of actin-based motility of Listeria and Shigella using pure proteins. Nature *401*, 613–616.
4. Akin, O., and Mullins, R.D. (2008). Capping protein increases the rate of actin-based motility by promoting filament nucleation by the Arp2/3 complex. Cell *133*, 841–851.
5. Bernheim-Groswasser, A., Wiesner, S., Golsteyn, R.M., Carlier, M.F., and Sykes, C. (2002). The dynamics of actin-based motility depend on surface parameters. Nature *417*, 308–311.
6. Dayel, M.J., Akin, O., Landeryou, M., Risca, V., Mogilner, A., and Mullins, R.D. (2009). In silico reconstitution of actin-based symmetry breaking and motility. PLoS Biol. *7*, e1000201.
7. van der Gucht, J., Paluch, E., Plastino, J., and Sykes, C. (2005). Stress release drives symmetry breaking for actin-based movement. Proc. Natl. Acad. Sci. USA *102*, 7847–7852.
8. Machesky, L.M., Mullins, R.D., Higgs, H.N., Kaiser, D.A., Blanchoin, L., May, R.C., Hall, M.E., and Pollard, T.D. (1999). Scar, a WASp-related protein, activates nucleation of actin filaments by the Arp2/3 complex. Proc. Natl. Acad. Sci. USA *96*, 3739–3744.
9. Michelot, A., Berro, J., Guérin, C., Boujemaa-Paterski, R., Staiger, C.J., Martiel, J.L., and Blanchoin, L. (2007). Actin-filament stochastic dynamics mediated by ADF/cofilin. Curr. Biol. *17*, 825–833.
10. Marchand, J.B., Kaiser, D.A., Pollard, T.D., and Higgs, H.N. (2001). Interaction of WASP/Scar proteins with actin and vertebrate Arp2/3 complex. Nat. Cell Biol. *3*, 76–82.
11. Michelot, A., Derivery, E., Paterski-Boujemaa, R., Guérin, C., Huang, S., Parcy, F., Staiger, C.J., and Blanchoin, L. (2006). A novel mechanism for the formation of actin-filament bundles by a nonprocessive formin. Curr. Biol. *16*, 1924–1930.
12. Cameron, L.A., Svitkina, T.M., Vignjevic, D., Theriot, J.A., and Borisy, G.G. (2001). Dendritic organization of actin comet tails. Curr. Biol. *11*, 130–135.
13. Vignjevic, D., Yarar, D., Welch, M.D., Peloquin, J., Svitkina, T., and Borisy, G.G. (2003). Formation of filopodia-like bundles in vitro from a dendritic network. J. Cell Biol. *160*, 951–962.
14. Cameron, L.A., Robbins, J.R., Footer, M.J., and Theriot, J.A. (2004). Biophysical parameters influence actin-based movement, trajectory, and initiation in a cell-free system. Mol. Biol. Cell *15*, 2312–2323.
15. Pantaloni, D., Boujemaa, R., Didry, D., Gounon, P., and Carlier, M.F. (2000). The Arp2/3 complex branches filament barbed ends: functional antagonism with capping proteins. Nat. Cell Biol. *2*, 385–391.
16. Berg, O.G., and von Hippel, P.H. (1985). Diffusion-controlled macromolecular interactions. Annu. Rev. Biophys. Biophys. Chem. *14*, 131–160.
17. Mogilner, A., and Oster, G. (1996). Cell motility driven by actin polymerization. Biophys. J. *71*, 3030–3045.